Ehrhart, M., Lienhart W., "Image-based dynamic deformation monitoring of civil engineering structures from long ranges", Proc. SPIE 9405, Image Processing: Machine Vision Applications VIII, 94050J (February 27, 2015); doi:10.1117/12.2075888; http://dx.doi.org/10.1117/12.2075888

Image-based dynamic deformation monitoring of civil engineering structures from long ranges

Matthias Ehrhart*, Werner Lienhart
Institute of Engineering Geodesy and Measurement Systems, Graz University of Technology, Steyrergasse 30, 8010 Graz, Austria

ABSTRACT

In this paper, we report on the vibration and displacement monitoring of civil engineering structures using a state of the art image assisted total station (IATS) and passive target markings. By utilizing the telescope camera of the total station, it is possible to capture video streams in real time with 10fps and an angular resolution of approximately 2″/px. Due to the high angular resolution resulting from the 30x optical magnification of the telescope, large distances to the object to be monitored are possible. The laser distance measurement unit integrated in the total station allows to precisely set the camera's focus position and to relate the angular quantities gained from image processing to units of length. To accurately measure the vibrations and displacements of civil engineering structures, we use circular target markings rigidly attached to the object. The computation of the targets' centers is performed by a least squares adjustment of an ellipse according to the Gauß-Helmert model from which the parameters of the ellipse and their standard deviations are derived. In laboratory experiments, we show that movements can be detected with an accuracy of better than 0.2mm for single frames and distances up to 30m. For static applications, where many video frames can be averaged, accuracies of better than 0.05mm are possible. In a field test on a life-size footbridge, we compare the vibrations measured by the IATS to reference values derived from accelerometer measurements.

Keywords: structural health monitoring, bridge vibrations, image assisted total station, pattern recognition, ellipse fit, Gauß-Helmert model, telescope camera

1. INTRODUCTION

Today, many large-scale civil engineering structures are permanently monitored to provide early warnings and to initiate counter actions from structural failure. This monitoring involves the investigation of the structure's vibration and displacement behavior. Vibration monitoring allows to analyze the frequencies included in the structure's oscillation and to identify the natural frequencies. If the forced vibration applied to a structure equals its natural frequency, the amplitude of the structure's oscillation rapidly increases[1],[2] which may cause a structural failure. It is thus important to know the natural frequencies in order to initiate counter actions (e.g. integration of damping systems) if possible forced vibrations are close the natural frequencies. For e.g. a footbridge, this means that additional damping is required if the step frequency of passengers corresponds to the bridge's natural frequency[2]. Vibration monitoring requires measurement equipment with high measurement rates and is traditionally done with accelerometers[2],[3],[4].

The displacement monitoring involves the long-term observation of the structure to investigate its movement due to diurnal (e.g. solar radiation) or annual (e.g. temperature variations) effects. It is also necessary for load testing which is done to validate the design of e.g. new bridges before they are approved for traffic[5]. The measurement equipment used for displacement monitoring requires a high temporal stability and should directly measure the displacements in units of length. Accelerometers are not feasible for this purpose. Although the displacements can theoretically be computed by double-integration of the accelerations over time, this does not work well in practice for long observation times and static loads[4],[6]. Traditional sensors for displacement monitoring are linear variable displacement transducers (LVDT) and dial gauges[4],[7]. Their major disadvantage is that they require stable, mechanical reference points close to the moving structure which is hard to establish in practice in some cases (e.g. on the top of a high-rise building or in the central section of a bridge). Therefore, total stations[8],[9] and Global Navigation Satellite Systems (GNSS) such as GPS[6],[10],[11],[12] are commonly used for the displacement monitoring of civil engineering structures and can also be utilized to investigate the

*matthias.ehrhart@tugraz.at; igms.tugraz.at

vibration behavior of the structures[6],[11],[13],[14],[15]. An advantage of using total stations and GNSS for monitoring purposes is that the reference points, which are necessary to assess the stability of the measurement system, are not needed to be located in the vicinity of the monitored structure. However, the usage of GNSS for structural health monitoring requires the measurement equipment (antenna and receiver including power supply) to be attached to the structure. Furthermore, errors on centimeter-level are possible due to multipath effects[12]. Using total stations requires special retro-reflective targets mounted on the structure to be monitored.

To overcome these limitations, different image-based approaches for vibration and displacement monitoring have been proposed[16],[17],[18],[19],[20]. To allow larger distances between the camera and the monitored structure, telescope lenses were used for the camera system[21],[22],[23]. These reported image-based systems use a single camera and are able to detect two-dimensional movements parallel to the sensor plane of the camera with up to 60fps[19],[20]. For the measurements it is sufficient to have simple target markings attached to the structure to be monitored. Some systems do not require any artificial target markings at all[18]. However, previously proposed methods have the common disadvantage that they require a stable point within the camera's field of view to control the stability of the setup. This is especially hard to establish for systems using telescope lenses due to their small field of view. Furthermore, the observed movements in the image (given in pixel) are related to units of length by comparison with a target of known size. This leads to systematic errors if the target is viewed from a skew angle which is not considered appropriately.

To overcome these problems we propose the use of total stations. Total stations are commonly utilized by surveyors to determine the 3D position of targets. A total station consists of a telescope rotatable about the vertical and the horizontal axis. These axes of rotation are motorized so that the telescope can be moved automatically to predefined positions. Total stations further comprise an electronic distance measurement (EDM) unit and a compensator which is used to ensure the accurate levelling of the instrument. The measured quantities are polar coordinates, i.e. the horizontal and vertical angle and the distance to the target.

Modern total stations are equipped with a camera integrated in the telescope and referred to as image assisted total stations (IATS). Currently, the camera is mainly used for documentation purposes but is a promising sensor for accurate measurements from long ranges since the angular resolution of the resulting image data benefits from the optical magnification of the telescope. The usage of IATS for vibration and displacement monitoring of civil engineering structures combines the advantages of conventional total station measurements (stability control by reading the telescope angles) and image-based methods (simple target markings). Furthermore, the observed pixel movements can be related to units of length using the measured distance to the monitored object. This makes the knowledge of the target size obsolete. The measured distance between the IATS and the object can also be used to automatically set the camera's focus position. Using IATS prototypes, experiments for the vibration monitoring of bridges were carried out[24],[25] whereat both approaches use active target markings requiring power supply.

In this paper, we present a new approach to utilize a state of the art IATS for the vibration and displacement monitoring from long ranges using passive target markings. We introduce the used measurement system (Section 2), describe our approach for the automated detection of the target markings (Section 3) and report on the system calibration (Section 4). Finally, we assess the achievable accuracies in laboratory investigations (Section 5.1), present measurement results gained from an experiment at a life-size footbridge (Section 5.2) and discuss the suitability of the system for practical measurement tasks (Section 6).

2. MEASUREMENT SYSTEM

The sensor of choice is the *MS50*[26] IATS (cf. Figure 1) from *Leica Geosystems*. The key component for our studies is the total station's on-axis camera, i.e. a camera that is located in the optical path of the telescope. The images are captured by a 2560px × 1920px CMOS sensor. The camera has a 30x optical magnification resulting from the telescope. The field of view is specified with 1.5°[26] (presumably image diagonal). From dividing this value by the image diagonal (in pixel) an angular resolution of 1.7″/px can be expected. However, in Section 4 we will show that the real value is slightly higher.

Compared to a standard camera with telescope lenses, the usage of an IATS has several advantages. The total station is able to determine the distance to an arbitrary object by an electronic distance measurement (for Leica MS50: up to

Ehrhart, M., Lienhart W., "Image-based dynamic deformation monitoring of civil engineering structures from long ranges", Proc. SPIE 9405, Image Processing: Machine Vision Applications VIII, 94050J (February 27, 2015); doi:10.1117/12.2075888; http://dx.doi.org/10.1117/12.2075888

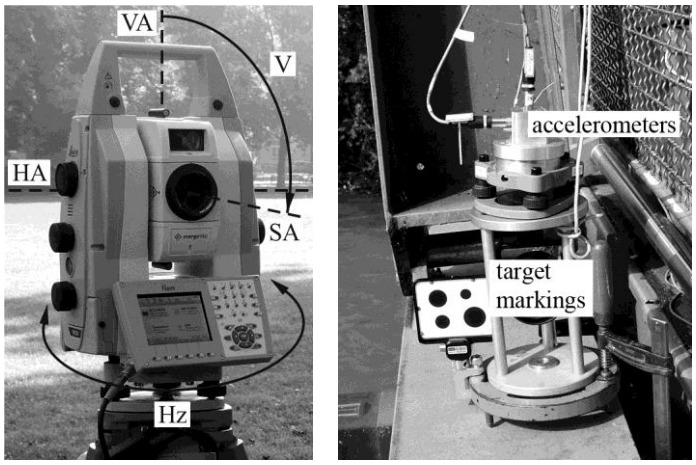

Figure 1. Left: MS50 total station from Leica Geosystems with camera located in the optical path of the telescope. The telescope axis coincides with the sighting axis (SA) of the total station. The telescope can be rotated about the vertical axis (VA) and the horizontal axis (HA). The measured quantities are the horizontal (Hz) and the vertical (V) angle and the distance (measured along SA) to a target. Right: passive target markings and accelerometers for reference measurements attached to the monitored structure.

2000m with a precision of 2mm + 2ppm[26]). With the known distance to the object it is possible to relate the angular quantities gained from image processing to units of length. Furthermore, the distance can be used to automatically set the telescope's focus motor position (autofocus). By reading the horizontal and vertical angles of the telescope (for Leica MS50: precision of 1″[26] and frequency of 20Hz) and by monitoring the tilt of the instrument with the internal compensator (for Leica MS50: precision of 0.5″[26] and frequency of 4Hz), it is possible to control the instrument's stability during the image data acquisition. Another major advantage is the total station's ability to automatically rotate its telescope to predefined positions. It is generally possible to access all sensors of the total station (e.g. distance measurement unit, compensator, motorization, etc.) from an external computer via software commands using the GeoCOM[27] interface.

The live stream of the video data captured by the total station can be read with 10fps on an external computer with a delay of approximately 2s. Although the total station's camera has a 2560px × 1920px CMOS sensor, the frames of the live stream are available only at 320px × 240px. It is thus left to the operator to decide whether the image data should be transmitted for the full field of view whereat the frames are downsampled from 2560px × 1920px to 320px × 240px. Alternatively, a reduced field of view with full image resolution (one pixel in the image corresponds to one pixel on the CMOS sensor) can be used. For our studies which require high accuracy, we decided to use the live stream at full image resolution and a reduced field of view.

Other manufacturers also offer instruments with comparable specifications. The *Topcon IS-3*[28] IATS is also equipped with an on-axis camera with a 30x optical magnification and would be a possible alternative to the Leica MS50. *Trimble* does also provide total stations with cameras but currently available instruments are only equipped with wide-angle cameras[29]. These cameras are not located within the optical path of the telescope and thus do not provide an optical magnification. They are therefore not applicable for high accurate measurements from long ranges.

In order to verify the suitability of IATS measurements for dynamic monitoring we equipped an object with circular target markings rigidly attached to the structure (cf. Figure 1). Basically, one target marking would be sufficient but we used several target markings with different sizes to investigate the influence of the target size on the results. These passive target markings are advantageous since they are very low-cost (simple printouts), do not require an external power supply and can easily be attached to the structure by simple sticking. For reference measurements of the bridge's vibration behavior, we also attached 3 accelerometers whereat they were oriented in vertical direction, across and along the bridge. This makes the application of our circular target markings appear a bit cumbersome (cf. Figure 1) but we emphasize that this due to the additional installation of the accelerometers.

Ehrhart, M., Lienhart W., "Image-based dynamic deformation monitoring of civil engineering structures from long ranges", Proc. SPIE 9405, Image Processing: Machine Vision Applications VIII, 94050J (February 27, 2015); doi:10.1117/12.2075888; http://dx.doi.org/10.1117/12.2075888

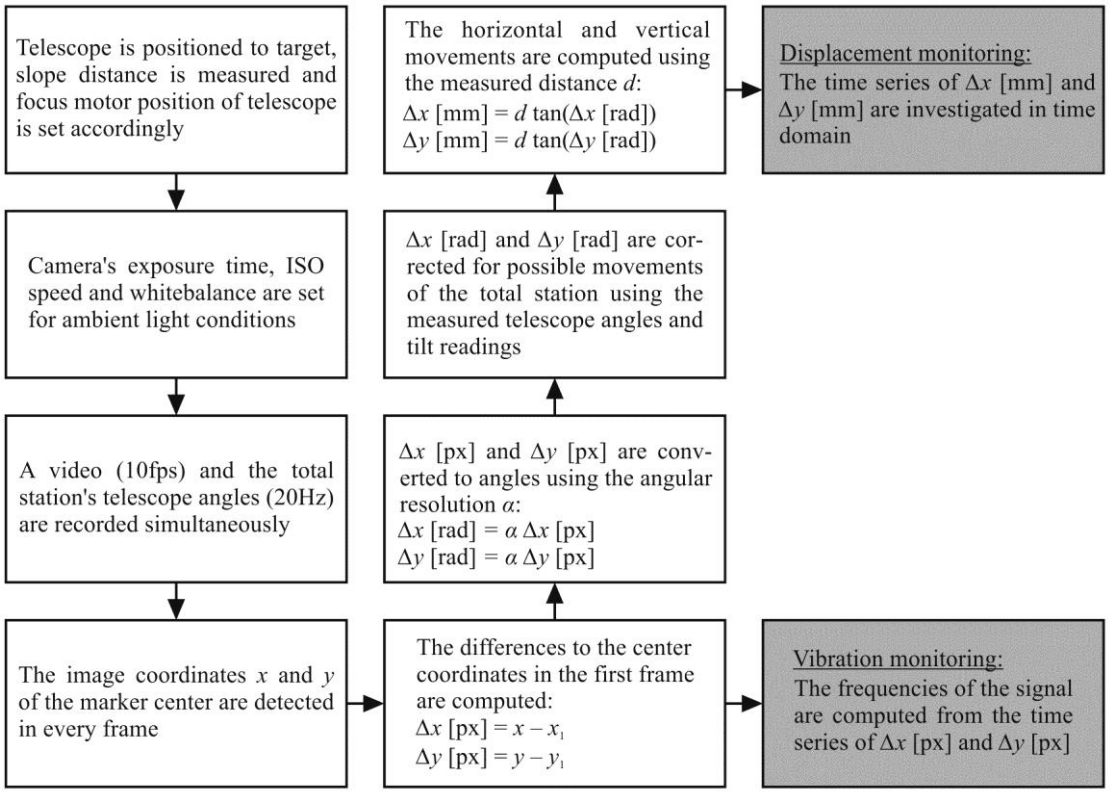

Figure 2. Workflow of our measurement system for the determination of vibrations and displacements of moving structures.

The workflow of the measurements with our system is outlined in Figure 2. The whole process can be automated and several targets on different positions on the structure can be monitored sequentially. A user interaction is only required to initially sight the targets on the structure and to set the camera's recording properties. For long-term monitoring, where different targets are observed in regular intervals, a manual sighting is only necessary in the first measurement epoch. Afterwards, the stored positions are used to automatically rotate the total station's telescope to the corresponding targets.

3. MARKER DETECTION

To obtain a representative value for the position of our circular target marking in the image, the center coordinates of the target have to be estimated. This can be done by a least squares fit of an ellipse based on the image coordinates of the marker's contour which first requires a detection of the marker by means of image processing.

Figure 3 illustrates the marker detection workflow. From the full field of view, only a detail of the frame, retaining the full image resolution (cf. Section 2), is transmitted to an external computer. The colored image is then converted to an 8 bit grayscale image with pixel values between 0 (black) and 255 (white). Afterwards, a threshold is applied converting the grayscale image to a binary image, i.e. each pixel value below the threshold is set to 0 and each pixel value above the threshold is set to 1. Finally, the image coordinates of the marker's contour are computed by border following[30].

Based on the detected contour coordinates of the circle (given with a resolution of 1px), we apply a least squares fit of an ellipse according to the Gauß-Helmert model[31],[32],[33]. The functional relationship between the observations (image coordinates x and y of the contour) and the unknown quantities (center x_0 and y_0, semi-axes a and b, rotation angle φ) is given by

Ehrhart, M., Lienhart W., "Image-based dynamic deformation monitoring of civil engineering structures from long ranges", Proc. SPIE 9405, Image Processing: Machine Vision Applications VIII, 94050J (February 27, 2015); doi:10.1117/12.2075888; http://dx.doi.org/10.1117/12.2075888

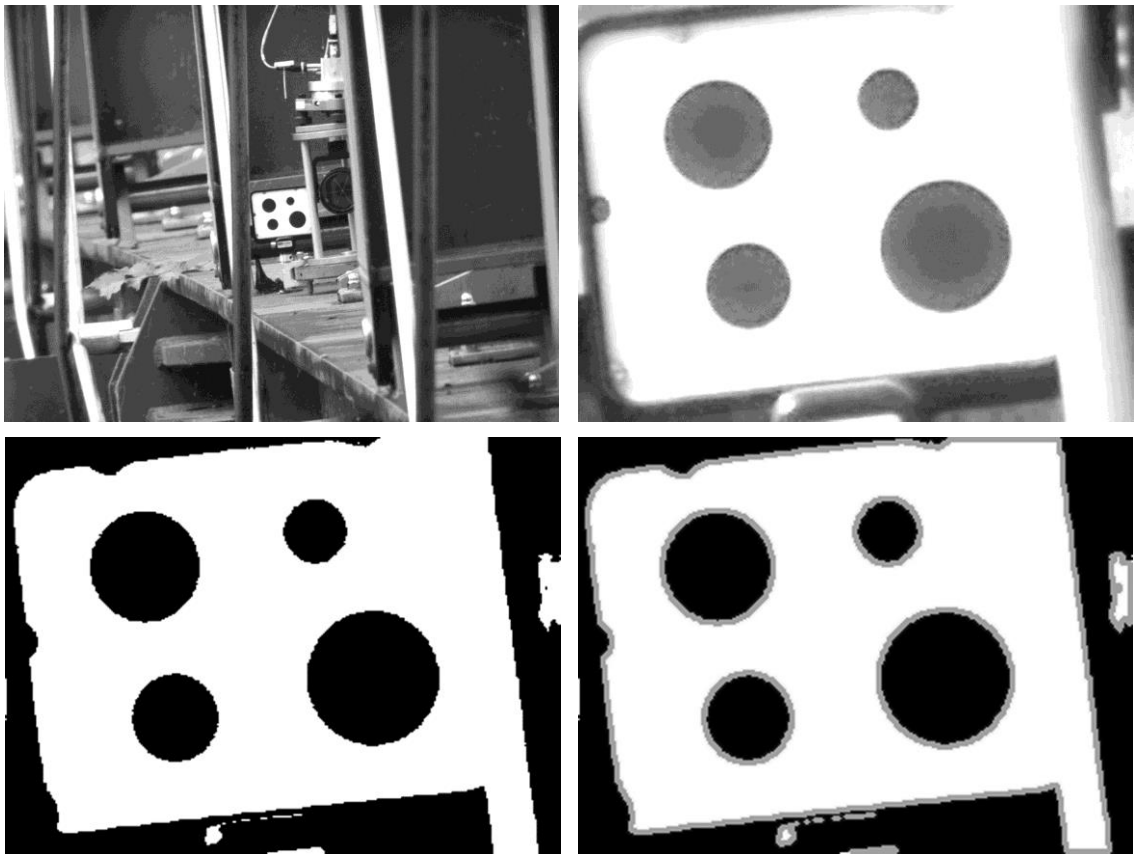

Figure 3. Illustration of the marker detection workflow with complete (top left) and reduced (top right) field of view, applied threshold (bottom left) and detected contours (bottom right).

$$\psi = \frac{x'^2}{a^2} + \frac{y'^2}{b^2} - 1 = 0 \tag{1}$$

with the auxiliary variables x' and y' which are computed by

$$\begin{bmatrix} x' \\ y' \end{bmatrix} = \begin{bmatrix} \cos\varphi & \sin\varphi \\ -\sin\varphi & \cos\varphi \end{bmatrix} \begin{bmatrix} x + v_x - x_0 \\ y + v_y - y_0 \end{bmatrix} \tag{2}$$

where v_x and v_y are the corrections to the original observations x and y.

The computations for the least squares adjustment according to the Gauß-Helmert model are performed iteratively where a $[n+5 \times n+5]$ matrix is inverted in every iteration. The dimension n is given by the number of contour points and the dimension 5 by the number of parameters to be estimated. In order to save computation time, good initial estimates for the ellipse parameters should be used. We therefore first estimate these parameters with a fast algorithm based on eigen-decomposition[34]. We also use these initial estimates to remove contours that do not belong to a circular marker (cf. Figure 3 bottom right). Based on the ratio of the semi-axes a and b and an empirically determined threshold only contours with $b/a > 0.2$ are further processed. We furthermore use the fast ellipse fit to detect outliers (normal distance to ellipse >2px) in the contour of the marker before we start the precise, iterative adjustment of the ellipse according to the Gauß-Helmert model. For the investigations in this paper, only the center coordinates x_0 and y_0 of the ellipse are of interest. We thus stop the iterative computation if the changes in the center coordinates are <0.01px. For our data, this typically occurred after 2 iterations.

For almost circular, evenly distributed contour coordinates in our data, the results of the center coordinates from the fast ellipse fit differ only by some 0.01px from the precise fit according to the Gauß-Helmert model. However, a major advantage of the Gauß-Helmert model is that it does not only yield the parameters of the ellipse as such but also their standard deviations. The standard deviations of the ellipse's center coordinates can be used as a measure of quality so that uncertain detections can be excluded from further computations.

Real images are always degraded by random noise and may be enhanced by using different image filters[35],[36],[37]. We thus tested the effects of Gaussian blur, median blur and bilateral filtering on the estimated marker center. However, none of the filters changed the results noticeably since the computation of the marker center is done by a least squares adjustment which, for normal distributed measurement data, finds the best estimate based on the minimum sum of squared errors[32],[38]. With only random noise in the measurement data (i.e. the contour coordinates), the least squares fit implicitly filters the noise and thus makes previous image filtering obsolete.

4. CALIBRATION OF THE MEASUREMENT SYSTEM

The measurement sensor of our system is a digital camera located in the optical path of the total station's telescope (cf. Section 2). As every measurements system used for the acquisition of highly accurate data, our system needs to be calibrated. The calibration of a camera generally involves the determination of its intrinsic parameters. These parameters are the image coordinates of the principal point (c_x and c_y), the focal lengths in horizontal and vertical direction (f_x and f_y) and an arbitrary number of coefficients to compensate for radial and tangential lens distortions (k_i and p_i).

The principal point is the intersection of the optical axis with the image sensor plane. For a pinhole camera model, the focal length is the distance between the camera center and the principal point. Usually two focal lengths are estimated during camera calibration to account for the fact that the pixels on the image sensor are non-square for some cameras[39]. Radial and tangential lens distortions result from an imperfect manufacturing of the lens and defects in the assembling of the camera[36] and distort the linear model for projecting points in the real world to the image plane[39]. Further information on the topic of camera calibration can be found in standard textbooks[36],[37],[39].

To obtain accurate intrinsic parameters, camera calibration is a time consuming task. We therefore investigate which parameters are really needed for the measurements described in this paper. Since displacement monitoring always involves the formulation of differences between different epochs, the constant image coordinates of the principal point will cancel out and are thus not needed to be known. For our long-range monitoring system and expected maximum object movements of a few centimeters, the image coordinates of the targets will only vary by some 10px. For e.g. an object movement of 20mm at a distance of 40m, the image coordinates change by 50px (on an image sensor with 2560px × 1920px, cf. Section 2). Distortion effects show a spatial regularity so that neighboring pixels are affected similarly. Accordingly, distortion effects will be reduced to a negligible extent when computing differences between objects located in similar regions on the image sensor. The frequencies included in a time series, which can be computed via Fourier analysis, are independent of the physical unit of the time series. This is due to the linear property of the Fourier transform[40] $F\{cf(t)\} = cF\{f(t)\}$ were a constant factor c may be applied before or after the transformation.

We thus can compute the frequencies included in the structure's oscillation from the raw image coordinates of the detected markers (cf. Figure 2). Consequently, no camera calibration is necessary for this purpose. However, for the investigation of the displacements in terms of a proper physical unit (e.g. millimeters), the knowledge of the camera's angular resolution is required. With this quantity, the movements in the image (given in pixels) can be computed to angular quantities which then can be related to units of length using the measured distance to the monitored object. The angular resolution expresses the size of one pixel of the image sensor in an angular quantity, i.e. it is the angle between two objects that are imaged on two neighboring pixel. For a pinhole camera model, the angular resolution α is related to the focal length f by $\tan\alpha = 1/f$.

The accurate knowledge of the angular resolution is crucial for the accurate calculation of displacements since object movements in the image (given in pixel) are multiplied by this value to compute angular quantities. As the object movements will amount to values up to several 10px, a small uncertainty in the value of the angular resolution translates to a large error in the computed angle. We thus calibrated this value in our temperature-controlled laboratory with a stable setup of the total station and the target. Similar to the *Theodolite-Sensor-Calibration*[41], we made use of the total station's ability to rotate its telescope about the vertical and the horizontal axis by precisely known angles (1″, cf. Section

2). Since the camera is located in the optical path of the telescope, it experiences the same rotations. For the determination of the angular resolution, we observed a circular target marking at a fixed position for different rotations of the telescope. For each telescope position, we recorded 10s of video data which results in 100 measurements for a frame rate of 10fps. For each frame, the target center was estimated according to Section 3. Simultaneously to the recording of the video, the telescope angles were streamed with 20Hz (cf. Section 2). Averaging the measurement series of the recorded angles improves the precision of the gained reference angle (precision of single angle measurement: 1″, cf. Section 2). To compute the angular resolution in horizontal and vertical direction, this procedure was carried out for horizontal and vertical rotations of the telescope.

Figure 4 exemplarily depicts the measurement data for horizontal rotations of the telescope. The angular resolution of the camera was computed as the slope of a straight line fitted to the data. Since both values (reference angles and image coordinates of the marker center) are affected by random errors, we used an orthogonal regression[32],[42] for the line fit. It would be possible to estimate additional parameters to compensate for radial distortion. As already pointed out, we expect object movements translating to a few 10px on the image sensor. We thus can neglect distortion effects and use a linear model for the estimation of the angular resolution of the camera.

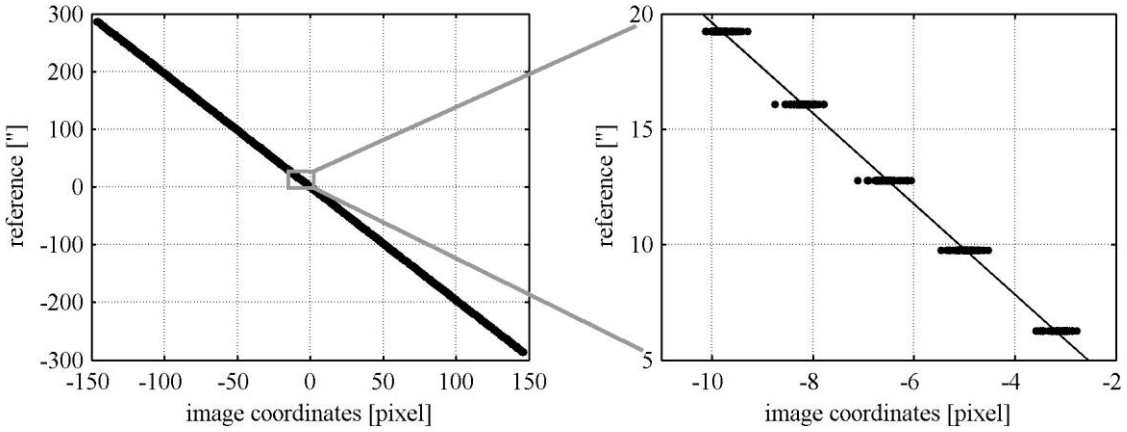

Figure 4. Relation between the image coordinates of the detected marker centers and reference angles for horizontal rotations of the telescope. Both quantities are centered by their mean values. The distance to the circular target marking with a diameter of 1mm was 6.339m. Left: complete measurement data. Right: detail with measurement series at each reference position and fitted regression line.

From the experiments, we estimated the angular resolutions and their standard deviations with $\alpha_{Hz} = 1.9627''/px$ (±0.0001px) in horizontal and $\alpha_V = 1.9632''/px$ (±0.0002px) in vertical direction. Although the estimates obviously differ in their absolute values, hypothesis testing[32],[38],[43],[44] showed that the difference is not significant on a 99% confidence level. This means that the pixels on the CMOS array can be considered square and that the two values can be averaged for a combined angular resolution of $\alpha = 1.9630''/px$ in horizontal and vertical direction.

The calibration with the proposed approach can be done within about one hour. This is important since the calibration parameters of cameras are known to vary over time[24] which requires periodic calibrations. With a fast, simple and automated calibration procedure, it is cost-effective to service the presented measurement system regularly.

5. EXPERIMENTAL RESULTS

To assess the accuracy potential of our measurement system for the vibration and displacement monitoring of civil engineering structures, we carried out two experiments. We evaluated the accuracy of the detected displacements in laboratory investigations (Section 5.1) and tested the capabilities for vibration monitoring in a field experiment at a life-size footbridge (Section 5.2).

Ehrhart, M., Lienhart W., "Image-based dynamic deformation monitoring of civil engineering structures from long ranges", Proc. SPIE 9405, Image Processing: Machine Vision Applications VIII, 94050J (February 27, 2015); doi:10.1117/12.2075888; http://dx.doi.org/10.1117/12.2075888

5.1 Accuracy of detected displacements

To evaluate the accuracy of the detected displacements, we investigated the computed values for accurately known reference movements under laboratory conditions. We therefore mounted our circular target markings on the linear positioning stage *Physik Instrumente M-410.DG* with a position repeatability of 2µm[45]. For the setup depicted in Figure 5, horizontal target movements are possible. For vertical movements, the linear positioning stage has to be aligned vertically.

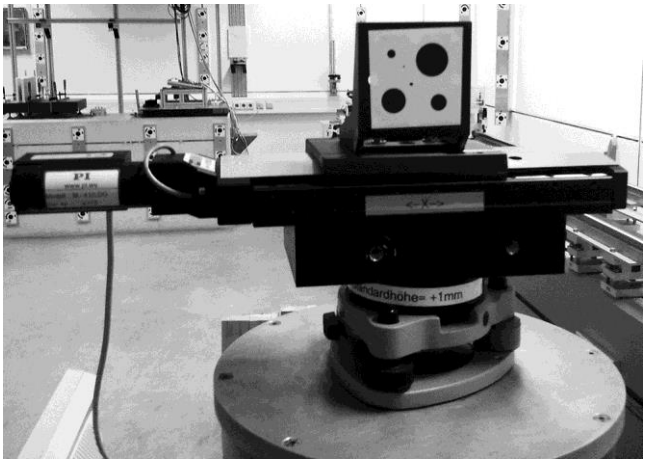

Figure 5. Linear positioning stage *Physik Instrumente M-410.DG* with a position repeatability of 2µm and circular target markings mounted onto its carriage.

For evaluating the accuracy of the detected displacements, the linear positioning stage was moved in steps of 0.25mm in a range of ±8mm. The stability of the setup was verified by measuring the zero position of the linear positioning stage at the beginning and the end of the experiment. This results in 67 reference positions. At each reference position a video was recorded for 10s which results in 100 frames for the recording with 10fps. Accordingly, 6700 frames were collected in total. The orthogonal orientation of the linear positioning stage's movement axis to the optical axis of the total station was ensured via autocollimation[43],[46]. To investigate the influences of the distance to the target and the target size, the experiments were carried out for distances of 6.2m, 12.5m, 18.8m and 31.4m and marker diameters of 1mm, 2mm, 5mm, 10mm, 15mm and 20mm.

The displacements detected with our system, which result from multiplying the pixel movements of the marker centers (cf. Section 3) by the angular resolution of the camera (cf. Section 4), were then compared to the reference movements of the linear positioning stage. For comparison, the detected displacements were converted from angles β to units of length b. This was done using the slope distance d measured by the total station and

$$b = d \tan \beta . \tag{3}$$

By rearranging Equation (3), the reference movements of the linear positioning stage can be converted to reference angles. Since the measurements in single images are the angles between different objects, investigating the residuals between the measured and the reference movements in arc seconds seems a natural choice. However, evaluating the perpendicular values of angles at certain distance is more descriptive sometimes. We thus provide both quantities (angles and perpendicular values) for the results shown in Table 1 and Figure 6.

Table 1 provides statistical information of the residuals between the movements detected with our system and the reference positions of the linear positioning stage. The averages refer to the mean values of the measurements at each position of the linear stage (100 frames). Additionally, the residuals of the single measurements (resulting from a single frame, 6700 frames in total) are investigated. Obviously, larger target markings have to be used for larger distances. At e.g. a distance of 31m a marker diameter of 2mm corresponds to approximately 7px in the image which is not sufficient for a precise ellipse fit. The statistical values of the residuals in terms of arc seconds are roughly constant for different distances. This is also shown by Figure 6 where we limit ourselves to suitable marker sizes.

Ehrhart, M., Lienhart W., "Image-based dynamic deformation monitoring of civil engineering structures from long ranges", Proc. SPIE 9405, Image Processing: Machine Vision Applications VIII, 94050J (February 27, 2015); doi:10.1117/12.2075888; http://dx.doi.org/10.1117/12.2075888

Table 1. Standard deviations and maximum values for the residuals of the averaged measurements at the reference positions (100 frames) and for the residuals of the single measurements (6700 frames in total) for different distances *d* and target diameters ø. The columns accented with gray background refer to suitable target sizes for the respective distance.

d **[m]**	**ø [mm]**	**residuals of averaged meas.**				**residuals of single meas.**			
		std.		**max.**		**std.**		**max.**	
		[″]	**[mm]**	**[″]**	**[mm]**	**[″]**	**[mm]**	**[″]**	**[mm]**
6.241	1	0.12	0.004	0.38	0.012	0.38	0.012	1.89	0.057
12.527	1	0.15	0.009	0.38	0.023	0.53	0.032	-1.92	-0.116
12.527	2	0.15	0.009	0.51	0.031	0.40	0.024	-1.67	-0.101
12.527	5	0.14	0.008	0.34	0.021	0.33	0.020	-1.54	-0.094
18.833	1	0.19	0.017	0.46	0.042	0.59	0.054	2.10	0.191
18.833	2	0.15	0.014	0.54	0.050	0.44	0.040	1.90	0.174
18.833	5	0.14	0.013	0.46	0.042	0.34	0.031	1.94	0.177
31.417	2	0.15	0.024	-0.46	-0.069	0.58	0.088	2.10	0.320
31.417	5	0.12	0.019	-0.38	-0.058	0.37	0.057	-2.00	-0.305
31.417	10	0.13	0.020	0.29	0.044	0.30	0.046	-1.51	-0.229
31.417	15	0.11	0.017	-0.29	-0.044	0.28	0.043	-1.18	-0.180
31.417	20	0.13	0.019	0.32	0.049	0.28	0.042	-1.24	-0.189

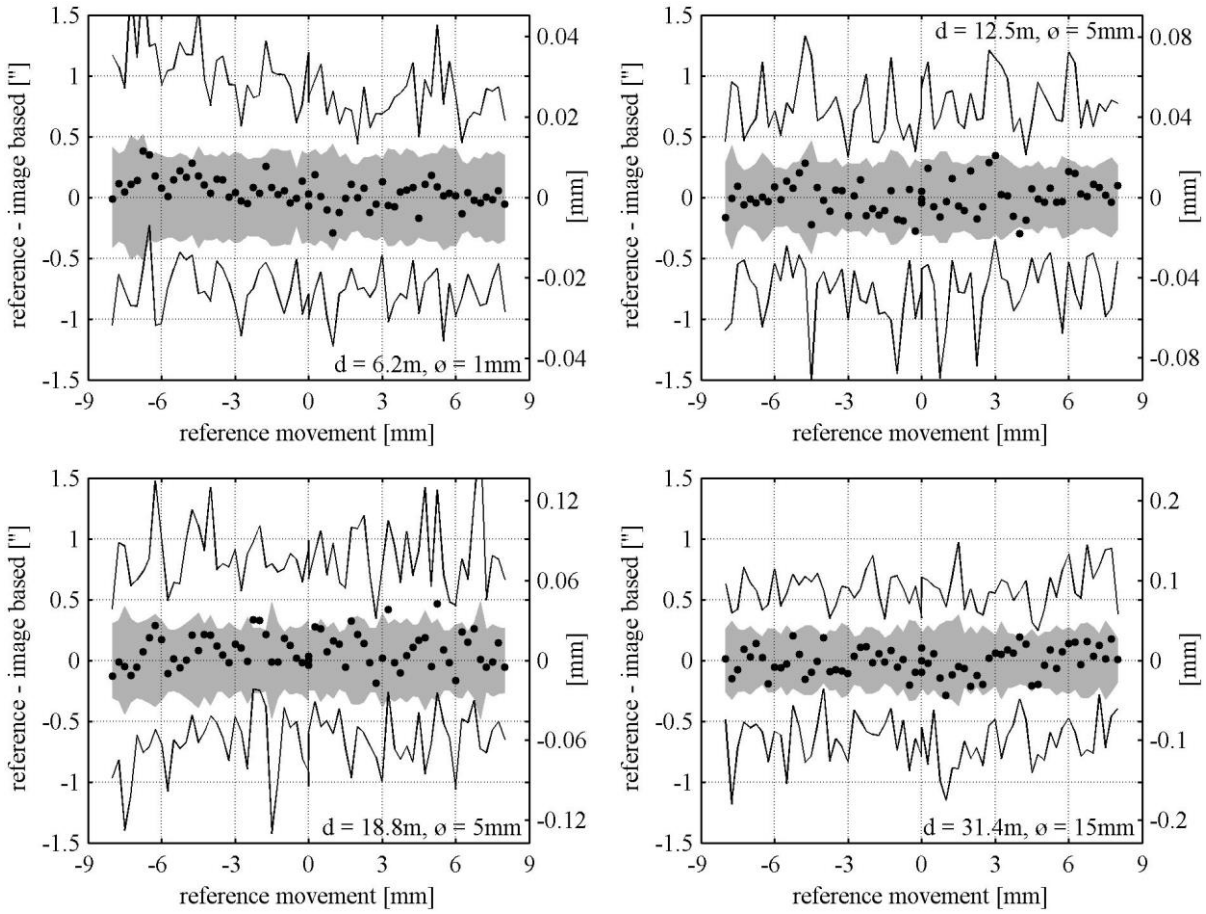

Figure 6. Residuals of the displacements computed from the detected target centers at different distances *d* and target diameters ø. The reference movements are gained from the positions of the linear positioning stage. With mean values (dots), standard deviations (gray area) and ranges (solid line) of the measurements at the reference positions.

The residuals in terms of millimeters increase almost linearly with the distance to the target (cf. Figure 7). For designing measurement campaigns, this is very helpful since the achievable accuracy of the movements measured with our system can be evaluated prior to the actual measurements. This can be done by relating the measurement accuracy (in arc seconds) to its perpendicular value using the approximate distance of the total station to the monitored object. For a distance of 31m, the errors of single measurements are <0.2mm and the errors for the averages of the measurements series (100 frames) are <0.05mm. At a distance of 6m, averaging the measurement series reveals a remarkable accuracy with errors <0.01mm.

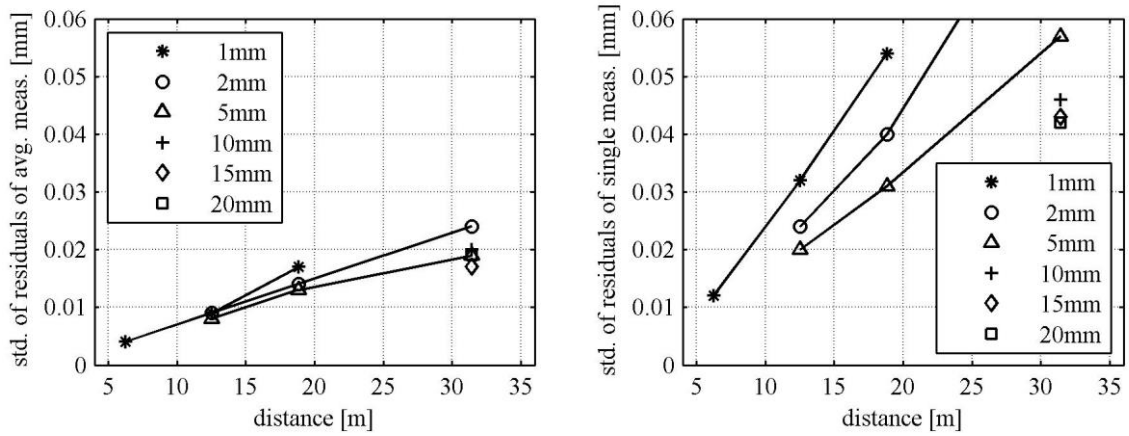

Figure 7. Standard deviations for the residuals of the averaged measurements (left) and for the residuals of the single measurements (right) for different distances and marker diameters.

5.2 Field experiment with vibration monitoring

To evaluate the ability of our system to measure the natural frequencies of civil engineering structures, we performed test measurements at the Augarten footbridge in Graz, Austria (cf. Figure 8). The distance of the total station to the passive target markings was about 39m. A similar distance (31m) was used for the test measurements in the laboratory where maximum errors of about 1″ occurred (cf. Table 1 and Figure 6). For the distance in the field experiment, this corresponds to a perpendicular value of 0.2mm. However, this value might be degraded due to turbulences of the air[25]. For reference measurements, the bridge was equipped with 3 accelerometers HBM B12/200[47] oriented in vertical direction, across and along the bridge. As depicted in Figure 8, we used different target sizes with diameters of 15mm, 20mm, 25mm and 30mm to evaluate the influence of the target size on the detected frequencies. The results presented here are based on the smallest target with a diameter of 15mm. It is noted again (cf. Section 2), that the somewhat cumbersome mounting of the target markings is due to the additional installation of the accelerometers and will be simplified for IATS measurements only.

In this paper, we only examine the vertical movements of the bridge. We emphasize that the focus of this paper is not on how to correctly identify the natural frequencies of this specific bridge but on evaluating the vibration measurements with a cost-effective, novel approach. For a correct identification of the natural frequencies, the structure needs to be excited. This can be done with an impact hammer, an electromagnetic shaker with variable frequencies[2] or by ambient vibration[3],[48]. In our experiment, we excited the bridge by two persons jogging over the bridge. The resulting time series are depicted in Figure 9.

Ehrhart, M., Lienhart W., "Image-based dynamic deformation monitoring of civil engineering structures from long ranges", Proc. SPIE 9405, Image Processing: Machine Vision Applications VIII, 94050J (February 27, 2015); doi:10.1117/12.2075888; http://dx.doi.org/10.1117/12.2075888

Figure 8. Augarten footbridge equipped with passive target markings and accelerometers for reference measurements.

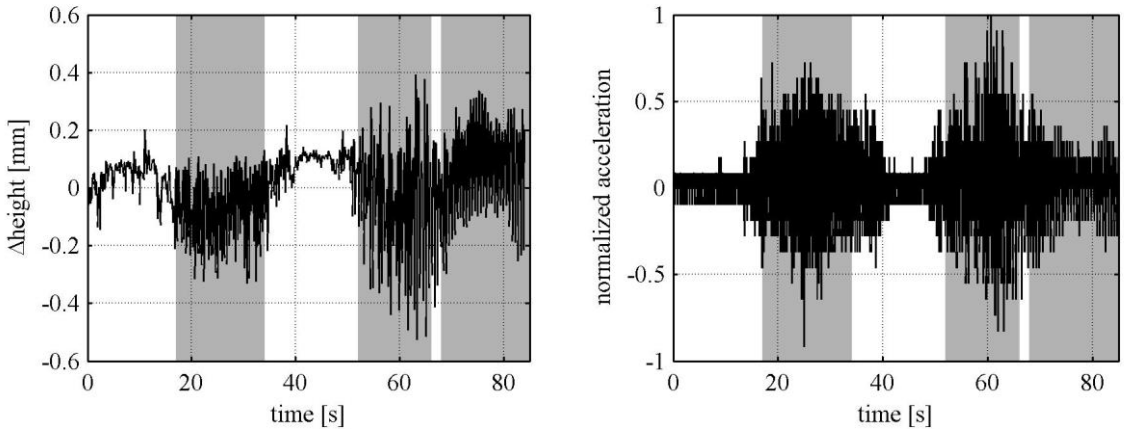

Figure 9. Vertical movements measured by the IATS (left) and measured accelerations (right) resulting from two persons jogging over the bridge. The gray areas mark the first and the second transition of the joggers and the post-pulse oscillation of the bridge.

One advantage of the measurements with the IATS is that the displacements of the bridge can be investigated in time domain. The IATS measurements reveal vertical movements of up to 0.5mm (cf. Figure 9). Further measurements of displacement monitoring with our system are reported in[49]. Using the accelerometer measurements, the displacements can theoretically be computed by double-integration of the accelerations over time. However, this does not work well in practice for long observation times and static loads[4],[6].

Figure 10 depicts the frequency responses of the footbridge for the time series highlighted in Figure 9. For the first transition of the joggers, a dominant frequency of 2.3Hz is visible. This value corresponds to the step frequency of the joggers and thus can be regarded as a forced vibration. The frequency is identified by the IATS (2.29Hz) and the accelerometer (2.30Hz). For the second transition, the step frequency of the joggers (2.3Hz) is visible again but the dominant frequency is 1.8Hz which presumably corresponds to the bridge's natural frequency. Again, this frequency is identified by the IATS (1.77Hz) and the accelerometer (1.78Hz). For the post-impulse oscillation of the bridge, which occurs after the joggers left the bridge, the natural frequency of 1.8Hz is visible where the IATS (1.81Hz) and the accelerometer (1.81Hz) yield the same results.

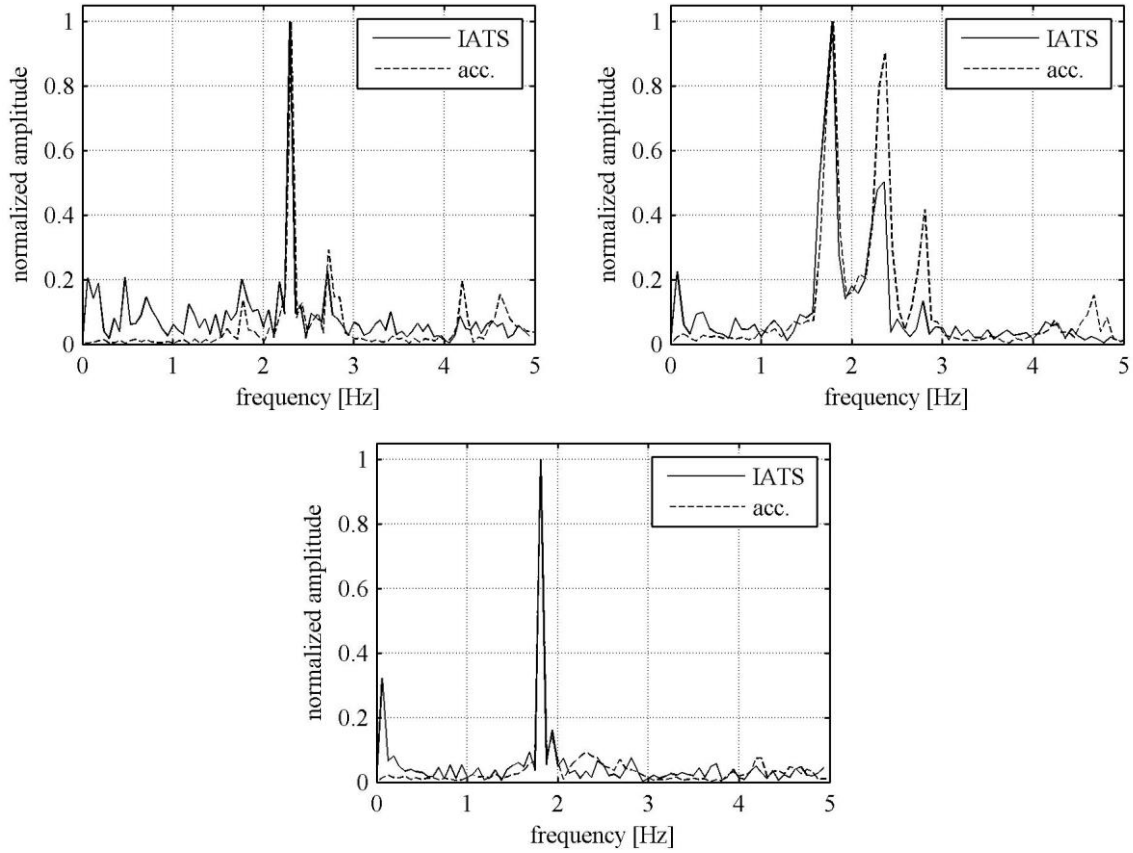

Figure 10. Amplitude spectral densities computed from measurements with IATS and accelerometer for the first and second transition of the joggers (top row) and the post-pulse oscillation of the bridge (bottom).

6. CONCLUSIONS

In this paper, we report on the vibration and displacement monitoring of civil engineering structures using a state of the art image assisted total station (IATS) and passive target markings. The core element of our measurements system is the total station's on-axis camera with an angular resolution of approximately 2″/px and a maximum frame rate of 10fps (cf. Section 2). In laboratory experiments we show, that the errors of the detected displacements from a distance of 31m are <0.2mm for single frames and <0.05mm for the average of a 10s video sequence (cf. Section 5.1). In a field experiment at a life-size footbridge and by comparison with accelerometer measurements, we demonstrate that the IATS is able to correctly identify the frequencies included in the structure's oscillation (cf. Section 5.2).

The shortcoming of the measurement system is the low frame rate of 10fps when transmitting the total station's live stream to an external computer. The camera of the used total station is able to capture videos with 20fps since it is possible to display the camera's live stream with 20fps via the total station's user interface[26]. Accordingly, the reduced frame rate of 10fps is probably due to the interface between the total station and an external computer and might be improved in future firmware releases and/or instrument series. By using a prototype of an IATS, frame rates up to 200fps are possible[25]. However, the critical natural frequencies f_i of footbridges in vertical direction are only $1.25\text{Hz} \leq f_i \leq 4.6\text{Hz}$[2] and therefore can already be identified with the used state of the art IATS.

The major advantage of the IATS is that it combines conventional total station measurements for displacement monitoring and accelerometer measurements for vibration analysis. Replacing the accelerometers and data processing units including power supply on the civil engineering structure by simple, passive target markings is especially beneficial in cases of limited access due to e.g. safety regulations. Another key feature of the proposed measurement system is its cost-effective calibration (cf. Section 4).

Ehrhart, M., Lienhart W., "Image-based dynamic deformation monitoring of civil engineering structures from long ranges", Proc. SPIE 9405, Image Processing: Machine Vision Applications VIII, 94050J (February 27, 2015); doi:10.1117/12.2075888; http://dx.doi.org/10.1117/12.2075888

REFERENCES

[1] Dukkipati, R. V. and Srinivas, J., [Textbook of mechanical vibrations], 2nd ed., 6th print., PHI Learning, New Delhi (2012).
[2] Heinemeyer, C., Butz, C., Keil, A., Schlaich, M., Goldack, A., Trometer, S., Lukić, M., Chabrolin, B., Lemaire, A., Martin, P. O., Cunha, A. and Caetano, E., "Design of Lightweight Footbridges for Human Induced Vibrations", European Commission - JRC Scientific and Technical Reports, JRC 53442, EUR 23984 EN (2009).
[3] Wenzel, H. and Pichler, D., [Ambient Vibration Monitoring], John Wiley & Sons, West Sussex, England (2005).
[4] Faulkner, B. C., Barton, F. W., Baber, T. T. and McKeel, W. T., "Determination of bridge response using acceleration data", Report No. FHWA/VA-97-R5, Virginia Department of Transportation (1996).
[5] The Institution of Civil Engineers, [Guidelines for the Supplementary Load Testing of Bridges], Thomas Telford Publications, London (1998).
[6] Celebi, M., "GPS in dynamic monitoring of long-period structures", Soil Dynamics and Earthquake Engineering 20, 477-483 (2000).
[7] Woodhouse, N. G., Robson, S. and Eyre, J. R., "Vision Metrology and Three Dimensional Visualization in Structural Testing and Monitoring", The Photogrammetric Record 16(94), 625-614 (1999).
[8] Radovanovic, R. S. and Teskey, W. F., "Dynamic monitoring of deforming structures: GPS versus robotic tacheometry systems", Proceedings of 10th FIG Symposium on Deformation Measurements, Orange, California, 61-70 (2001).
[9] Kuhlmann, H. and Gläser, A., "Investigation of new Measurement Techniques for Bridge Monitoring", 2nd Symposium on Geodesy for Geotechnical and Structural Engineering, Berlin, Germany, 123-132 (2002).
[10] Im, S., Hurlebaus, S. and Kang, Y., "Summary Review of GPS Technology for Structural Health Monitoring", Journal of Structural Engineering 139(10), 1653-1664 (2013).
[11] Nakamura, S., "GPS Measurement of Wind-Induced Suspension Bridge Girder Displacements", Journal of Structural Engineering 126(12), 1413-1419 (2000).
[12] Wieser, A. and Brunner, F. K., "Analysis of Bridge Deformations using Continuous GPS Measurements", 2nd Conference of Engineering Surveying, Bratislava, Slovakia (2002).
[13] Cosser, E., Roberts, G. W., Meng, X. and Dodson, A. H., "Measuring the dynamic deformation of bridges using a total station", Proceedings of 11th FIG Symposium on Deformation Measurements, Santorini, Greece (2003).
[14] Lekidis, V., Tsakiri, M., Makra, K., Karakostas, C., Klimis, N. and Sous, I., "Evaluation of dynamic response and local soil effects of the Evripos cable-stayed bridge using multi-sensor monitoring systems", Engineering Geology 79(1-2), 43-59 (2005).
[15] Psimoulis, P. A. and Stiros, S. C., "Measurement of deflections and of oscillation frequencies of engineering structures using Robotic Theodolites (RTS)", Engineering Structures 29(12), 3312-3324 (2007).
[16] Wahbeh, A. M., Caffrey, J. P. and Masri, S. F., "A vision-based approach for the direct measurement of displacements in vibrating systems", Smart Materials and Structures 12(5), 785-794 (2003).
[17] Schwarz, W., "Vermessungen im Sub-Millimeter-Bereich", Allgemeine Vermessungs-Nachrichten 8-9, 341-350, (2007).
[18] Caetano, E., Silva, S. and Bateira, J., "A vision system for vibration monitoring of civil engineering structures", Experimental Techniques 35(4), 74-82 (2011).
[19] Choi, H. S., Cheung, J. H., Kim, S. H. and Ahn, J. H., "Structural dynamic displacement vision system using digital image processing", NDT&E International 44(7), 597-609 (2011).
[20] Kim, S. W. and Kim, N. S., "Multi-point Displacement Response Measurement of Civil Infrastructures Using Digital Image Processing", Procedia Engineering 14, 195-203 (2011).
[21] Olaszek, P., "Investigation of the dynamic characteristic of bridge structures using a computer vision method", Measurement 25(3), 227-236 (1999).
[22] Lee, J. J. and Shinozuka, M., "Real-Time Displacement Measurement of a Flexible Bridge Using Digital Image Processing Techniques", Experimental Mechanics 46, 105-114 (2006).
[23] Martins, L. L., Rebordão, J. M. and Ribeiro, A. S., "Conception and development of an optical methodology applied to long-distance measurement of suspension bridges dynamic displacement", Journal of Physics: Conference Series 459 (2013).

[24] Bürki, B., Guillaume, S., Sorber, P. and Oesch, H.P., "DAEDALUS: A Versatile Usable Digital Clip-on Measuring System for Total Stations", 2010 International Conference on Indoor Positioning and Indoor Navigation (IPIN), Zurich, Switzerland (2010).
[25] Wagner, A., Wasmeier, P., Reith, C., Wunderlich, T., "Bridge Monitoring by Means of Video-Tacheometer - A Case Study", Allgemeine Vermessungs-Nachrichten 8-9, 283-292 (2013).
[26] Leica Geosystems AG, "Leica MS50/TS50/TM50 User Manual", Version 1.1.1 (2013).
[27] Leica Geosystems AG, "Leica Nova MS50 GeoCOM Reference Manual", Version 5.50 (2014).
[28] Topcon Corp., "Imaging Station Instruction Manual" (2011).
[29] Joyce, K., Koehler, M. and Vogel, M., "Trimble VISION white paper" (2012).
[30] Suzuki, S. and Abe, K., "Topological Structural Analysis of Digitized Binary Images by Border Following", Computer Vision, Graphics, and Image Processing 30, 32-46 (1985).
[31] Grafarend E. W., [Linear and nonlinear models: fixed effects, random effects, and mixed models], de Gruyter, Berlin (2006).
[32] Niemeier, W., [Ausgleichungsrechnung], 2. Auflage, de Gruyter, Berlin (2008).
[33] Lenzmann, L. and Lenzmann, E., "Strenge Auswertung des nichtlinearen Gauß-Helmert-Modells", Allgemeine Vermessungs-Nachrichten 2, 68-73 (2004).
[34] Fitzgibbon, A. W., Pilu, M. and Fisher, R. B., "Direct least squares fitting of ellipses", Proceedings of the 13th International Conference on Pattern Recognition, 253-257 (1996).
[35] Gonzales, R. C. and Woods R. E., [Digital Image Processing], 2nd ed., Prentice Hall, New Jersey (2002).
[36] Bradski, G. and Kaehler, A., [Learning OpenCV], O'Reilly, US (2008).
[37] Szeliski, R., [Computer Vision: Algorithms and Applications], Springer, London (2011).
[38] Brand, S., [Data analysis], 3. ed., Springer, New York (1999).
[39] Hartley, R. and Zisserman, A., [Multiple View Geometry in Computer Vision], 2nd ed., Cambridge University Press, Cambridge (2003).
[40] Andrews, L. C. and Phillips R. L., [Mathematical techniques for engineers and scientists], SPIE Press, Bellingham (2003).
[41] Walser, B., "Development and Calibration of an Image Assisted Total Station", PhD thesis, ETH Zurich (2004).
[42] Deming, W. E, [Statistical adjustment of data], 1st ed., 4th print., Wiley, New York (1948).
[43] Möser, M., Hoffmeister, H., Müller, G., Staiger, R., Schlemmer, H. and Wanninger, L., [Handbuch Ingenieurgeodäsie: Grundlagen], 3. Auflage, Wichmann, Berlin (2000).
[44] Ghilani, C. D. and Wolf, P. R., [Adjustment Computations: Spatial Data Analysis], 4th ed., John Wiley & Sons, New Jersey (2006).
[45] Physik Instrumente (PI) GmbH & Co. KG, "MP 35E User Manual", Release: 3.3.3 (2008).
[46] Reilly, J. P., "Optical Tooling", In: The Surveying Handbook, 2nd ed., Chapman & Hall (1995).
[47] HBM Mess- und Systemtechnik GmbH, "Acceleration Transducer B12 Mounting Instructions", Version 17.2.2000 (2000).
[48] Sohn, H., Farrar, C. R., Hemez, F. M., Shunk, D. D., Stinemates, D. W. and Nadler, B. R., "A Review of Structural Health Monitoring Literature: 1996-2001", Los Alamos National Laboratory Report LA-13976-MS (2003).
[49] Ehrhart, M. and Lienhart, W., "Development and evaluation of a long range image-based monitoring system for civil engineering structures", Proc. SPIE 9437, paper accepted for publication (2015).